Available online at www.sciencedirect.com
SCIENCE DIRECT
Polymer 46 (2005) 3419–3424
polymer
www.elsevier.com/locate/polymer

Effect of solvent solubility parameter on SWNT dispersion in PMMA

Jing Liu, Tao Liu, Satish Kumar*

School of Polymer, Textile and Fiber Engineering, Georgia Institute of Technology, Atlanta, GA 30332, USA

Received 16 September 2004; received in revised form 18 February 2005; accepted 28 February 2005
Available online 21 March 2005

Abstract

SWNT were dispersed in PMMA in eight different solvents with varying three dimensional solubility parameters. Results show that for achieving good dispersion, the polar component (δ_p) of the solubility parameter is most important, while the other components, namely dispersive and hydrogen bonding (δ_d and δ_h), or the total solubility parameter (δ_t) do not appear to be so critical. The best SWNT/PMMA dispersion was achieved in nitromethane, the most polar solvent used in this study. SWNT/PMMA samples exhibiting different degrees of dispersion have been studied using Raman spectroscopy. The intensity variations in the Raman radial breathing mode, as well as changes in the tangential (G) and overtone of the disorder (G′) band peak positions are consistent with the qualitative dispersion observations obtained from optical and scanning electron microscopy.

Keywords: Dispersion; Nanotube; PMMA

1. Introduction

Due to their exceptional electronic and mechanical properties [1], interest in single wall carbon nanotubes (SWNT's) has increased steadily since, their discovery in 1993 [2,3]. They are considered to be ideal candidates for developing functional and structural polymer/SWNT composites [4]. It has been shown that the incorporation of only a few percent of SWNT into many polymers leads to significant improvement in mechanical [5–8] and electrical [9,10] properties. To fully explore their reinforcing potential, uniform SWNT dispersion is necessary. In addition, SWNT exfoliation and orientation are also important [11].

Raman spectroscopy is a powerful and non-destructive method to characterize SWNT and SWNT based materials. The typical Raman spectrum of SWNT includes four main features: the tangential G band (near 1600 cm^{-1} and derived from the graphite-like in-plane vibration mode), the disorder induced D band (around 1300 cm^{-1}), the G′ band (at about 2600 cm^{-1} and it is generally considered to be the overtone of D band), and the low-frequency (generally in the 200–500 cm^{-1} range) radial breathing mode (RBM), which corresponds to the collective in-phase radial displacement of the carbon atoms [12]. The position of RBM is inversely proportional to the nanotube diameter and is frequently used to characterize the diameter distribution in a given SWNT sample. The intensity of the RBM bands depends on the laser excitation energy (E_{laser}) according to the resonance theory. It reaches its maximum intensity when E_{laser} matches the energy separation E_{ii} between the Van Hove singularities (VHS's) in the nanotube electronic density of states (DOS) [13]. Raman spectroscopy is also very effective for monitoring carbon nanotube deformation. The position of both G and G′ bands downshift under a tensile strain and up shift upon the application of compression or with pressure [14–17]. SWNT Raman modes shift to lower wave numbers with increasing temperature and G band has a larger temperature co-efficient than the RBM bands [18].

In this paper, we report a SWNT dispersion study in PMMA in eight different solvents with varying solubility parameters. The dispersion was characterized by optical and scanning electron microscopy. The solvents and their three-dimensional solubility parameter values are listed in Table 1. All the composite samples have been analyzed using Raman spectroscopy.

* Corresponding author. Tel.: +1 404 8947550; fax: +1 404 8948780.
E-mail address: satish.kumar@ptfe.gatech.edu (S. Kumar).

0032-3861/$ - see front matter © 2005 Elsevier Ltd. All rights reserved.
doi:10.1016/j.polymer.2005.02.086

Table 1
Solubility parameters of various solvents and PMMA [26]

Name	Molecular formula	δ_d (MPa$^{0.5}$)	δ_p (MPa$^{0.5}$)	δ_h (Mpa$^{0.5}$)	δ_t (MPa$^{0.5}$)
Toluene	C_7H_8	18.0	1.4	2.0	18.2
Methylene chloride	CH_2Cl_2	18.2	6.3	6.1	20.3
Methyl ethyl ketone	$CH_3COCH_2CH_3$	16.0	9.0	5.1	19.0
Acetone	CH_3COCH_3	15.5	10.4	7.0	20.1
Formic acid	HCOOH	14.3	11.9	16.6	25.0
N,*N*-Dimethylformamide	$HCON(CH_3)_2$	17.4	13.7	11.3	24.8
Acrylonitrile	H2C=CHCN	16.5	17.4	6.8	24.8
Nitromethane	CH_3NO_2	15.8	18.8	5.1	25.1
PMMA	$(CH_2C(CH_3)CO_2CH_3)_n$	18.6	10.5	7.5	22.7

δ_t: total solubility parameter, which is defined as: $\delta_t^2=\delta_d^2+\delta_p^2+\delta_h^2$, δ_d dispersive contribution, δ_p polar contribution, δ_h hydrogen bonding contribution.

2. Experimental

HiPCO™ nanotubes received from Carbon Nanotechnologies, Inc., were used without purification (Lot # R0231 and 35 wt% metal catalyst). PMMA ($\bar{M}_w = 95,000–150,000$ g/mol) was obtained from Cyro industries and was used as received. All solvents were purchased from Aldrich or from Fisher Scientific and were also used as received. SWNTs (10 mg) dispersed in 30 ml solvent were sonicated (the sonicator: Branson water bath sonicator by Smithkline Company, model B-22-4, power 125 W, frequency 43 KHz) for 70 h at room temperature (water circulation was used in the bath to maintain the bath temperature at 23 °C). PMMA (90 mg) was added to this dispersion, followed by sonication for another 5 h. The dispersion was poured on to a glass plate, and the solvent was allowed to evaporate in the hood over several days. The resulting SWNT weight fraction in PMMA was 10 wt%. LEO 1530 field emission scanning electron microscope was used to characterize the morphology of the SWNT/PMMA composite films, and all the samples were coated with gold. The Raman spectra were collected on Holoprobe Research Raman microscope made by Kaiser Optical Systems, Inc., using 785 nm excitation wavelength ($E_{laser}=1.58$ eV). The laser spot diameter was a few micrometers and the resolution of the Raman spectrometer was 1 cm^{-1}. For each composite film, Raman spectrum was collected at different positions using an exposure time of 1 min or exposure time of 1 s with 100 accumulations to minimize heating effect.

3. Results and discussion

SWNT/PMMA dispersions are optically homogeneous when processed from nitromethane, acrylonitrile, and *N*,*N*-dimethylformamide, while other five solvents (toluene, methylene chloride, methyl ethyl ketone, acetone, and formic acid) resulted in heterogeneous dispersion.

Optical micrographs of the PMMA/SWNT dispersions in nitromethane and in methyl ethyl ketone are given in Fig. 1 as examples of homogeneous and heterogeneous dispersions, respectively. Scanning electron micrographs in Fig. 2 show that composites processed from methyl ethyl ketone and methylene chloride are phase separated. However, the rope diameter of the pristine SWNT as well as in the composite samples processed from various solvents, measured from scanning electron micrographs using the Mat Lab software, were all the same (26 ± 3 nm).

Fig. 2 also shows that the composite processed from nitromethane is more homogeneous than the one from *N*,*N*-dimethylformamide, In fact, of all the eight solvents, the composite processed from nitromethane appear to be the most homogeneous. These observations clearly suggest that solvents do play an important role in obtaining uniform SWNT dispersion in PMMA. From the SWNT/PMMA dispersion study, it was observed that when solvent polar solubility parameter component (δ_p) was higher than the corresponding δ_p value of the polymer, dispersion tended to be more homogeneous. While the total solubility parameter (δ_t), as well as the dispersive component (δ_d) and hydrogen bonding component (δ_h) do not appear to play that significant role in SWNT dispersion.

SWNTs are hydrophobic non-polar rigid-rods. Molecular dynamics simulation suggests continuous and spontaneous filling of a non-polar carbon nanotube with a one-dimensionally ordered chain of water molecules [19]. There may be an ordered arrangement of polar solvents around non-polar SWNTs and the extent of solvent penetration in the interstices of the SWNT bundle may increase with solvent polarity. The presence of this solvent may become the driving force for the polymer penetration, resulting in good SWNT dispersion.

PMMA/SWNT composites have been studied using Raman spectroscopy to see if differences in SWNT dispersion give a Raman signature. For this purpose, two types of samples were prepared. The first type of samples was dried in the hood for several days. The second type of samples were prepared by heating the hood dried samples in differential scanning calorimetry (DSC) from 25 to 150 °C at 5 °C/min and then cooling at the same rate to room temperature, in order to relax any thermal strains in the sample as well as to ensure the removal of any residual solvent. G band shift as a function of $\Delta\delta_p(\delta_{p\text{-solvent}}-\delta_{p\text{-PMMA}})$ is

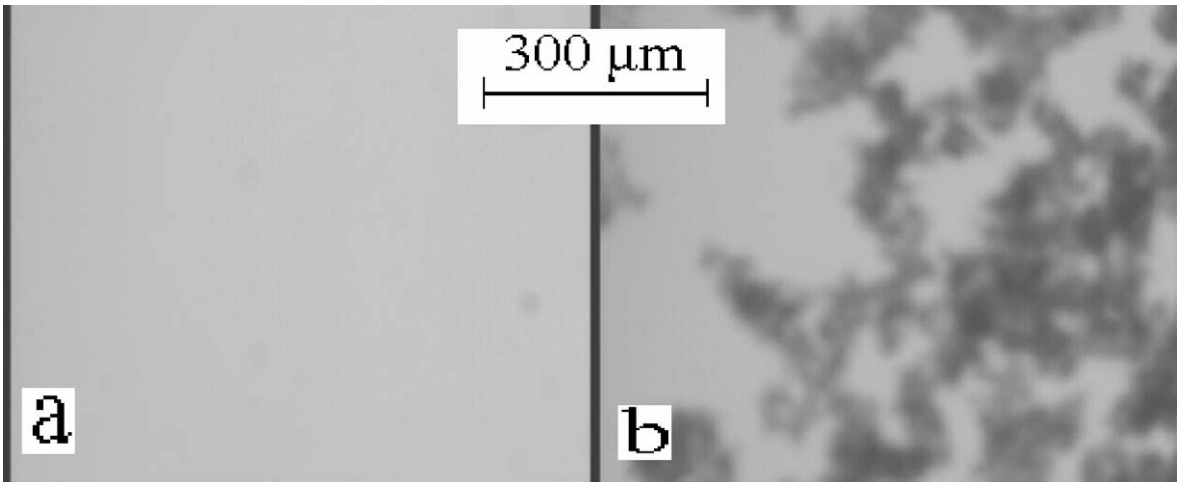

Fig. 1. Optical micrograph of (a) SWNT/PMMA/nitromethane and (b) SWNT/PMMA/methyl ethyl ketone dispersion.

plotted in Fig. 3. G band of SWNT powder was observed at 1589.5 cm^{-1} while it shifted to higher wave number for PMMA/SWNT composites processed from *N*,*N*-dimethylformamide, acrylonitrile, and nitromethane. No significant change was obtained in the G-band position for five solvents (toluene, methylene chloride, and methyl ethyl ketone, acetone and formic acid) giving optically heterogeneous dispersion, when exposure time of 1 s with 100

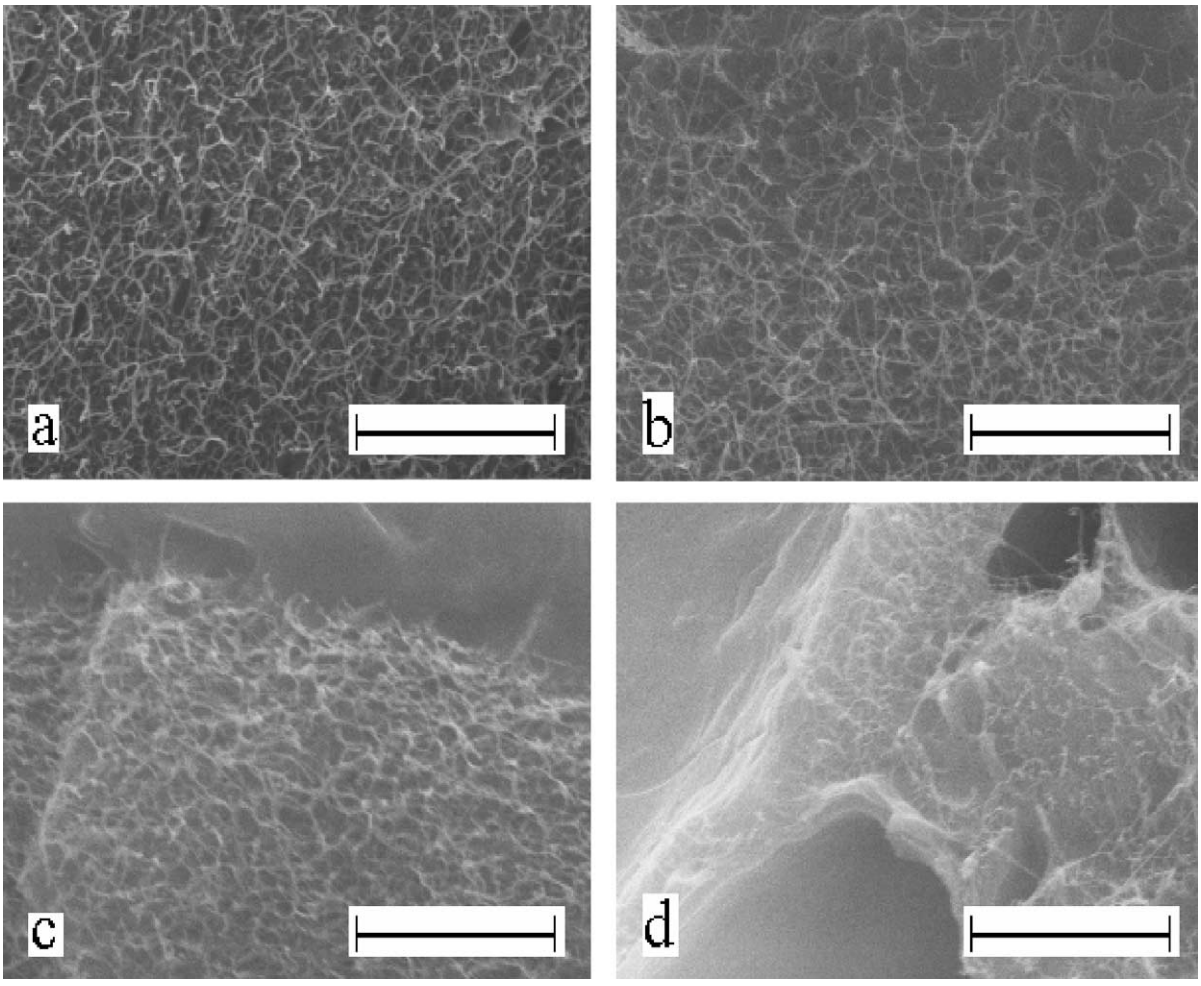

Fig. 2. Scanning electron micrograph of the PMMA/SWNT composite fracture surfaces. Solvents for (a) nitromethane, (b) *N*,*N*-dimethylformamide, (c) methyl ethyl ketone, and (d) methylene chloride. Scale bar is 2 μm.

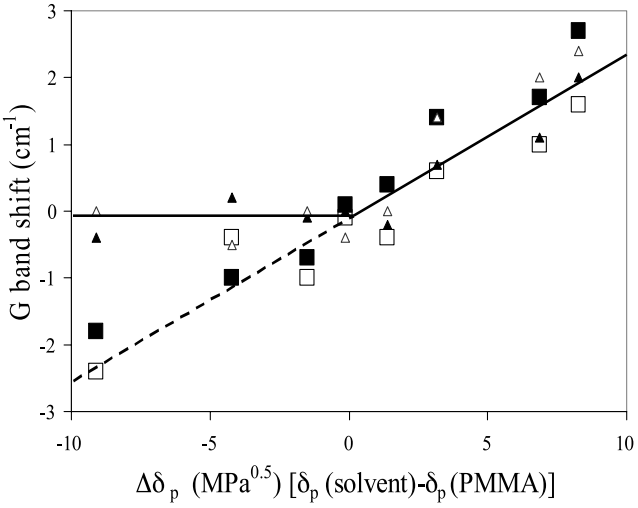

Fig. 3. G band shift in PMMA/AWNT composites processed in different solvents as a function of $\Delta\delta_p$ (open squares: thermally treated samples and laser exposure time 1 min during Raman experiment. Solid squares: air dried samples and laser exposure time 1 min. Open triangles: thermally treated samples and laser exposure time 1 s with 100 accumulations. Solid triangles: air dried samples and exposure time 1 s with 100 accumulations).

accumulations was used for collecting the Raman spectra. For heterogeneous samples G band downshifted when collection time for the Raman spectra was 1 min. This down shift was a result of sample heating due to prolonged exposure (1 min) to laser in heterogeneous samples while short exposure times (1 s) did not result in sample heating and hence no change in G band position. By comparison, for the samples exhibiting homogeneous SWNT distribution, G-band displacement was the same for both laser exposure times of 1 min and 1 s (100 accumulations). This is a result of better heat dissipation due to homogeneous SWNT dispersion. Thus in Fig. 3, dashed line represents heating effect while solid line is G band shift resulting from differences in SWNT dispersion in PMMA processed from different solvents. If δ_p of the solvent is less than that of the PMMA, the G band position remains the same as that for SWNT powder, however, if δ_p of the solvents is higher than that of PMMA, G band up shifts in proportion to $\Delta\delta_p(\delta_{p\text{-solvent}} - \delta_{p\text{-PMMA}})$.

G band shift for both the air-dried and thermally treated PMMA/SWNT composite samples was the same, indicating the absence of thermal strains. G band up shift for higher solvent δ_p values indicate compressive strain on SWNT or bundles.

Using the SWNT G band shift in Fig. 3, and the G band shift constant [17] of 8.7 cm^{-1}/GPa, about 0.25 GPa compressive stress is predicted on SWNT in PMMA/SWNT composite processed from nitromethane. Sample heating decreases the carbon–carbon bond force constant, and results in G and RBM band down shifts [20]. Temperature co-efficient of G band (~ -0.038 cm^{-1}/K) is higher than that for the RBM band (~ -0.013 cm^{-1}/K) [21]. In qualitative agreement with this observation, for 1 min exposure time, the difference between RBM peak positions for PMMA/SWNT samples processed from nitromethane and toluene is about 0.7 cm^{-1} wave number, while for the G band this difference is more than 4 cm^{-1} wave numbers. For the toluene processed film (data in Fig. 3), temperature increase of about 50 K is predicted in the Raman experiment for the 1 min exposure time using G band temperature co-efficient of ~ -0.038 cm^{-1}/K. For 1 min exposure, temperature effect dominates the $\Delta\delta_p$ less than zero region, and dispersion induced compressive strain effect dominates the $\Delta\delta_p$ greater than zero region.

Fig. 4 gives the G′ band shift of the composites as a function of $\Delta\delta_p$. As the case for G band, G′ band shift also increases with $\Delta\delta_p$ and is also a result of compressive strains on the SWNT in the composite. The composites processed from nitromethane has the largest G′ shift, by about 15–20 cm^{-1} and with absolute value as high as 2591 cm^{-1}.

The Raman spectra in RBM region for the HiPCO™ SWNT and for the PMMA/SWNT composites processed from toluene and nitromethane are plotted in Fig. 5. RBM peak position is not significantly affected by the strains in the film [22]. Small variations in the relative RBM intensities were observed when spectra were obtained at different positions on the sample. For SWNT powder and eight composites films, the low-frequency Raman spectra were all fitted with six Lorentzian components located at 203, 226, 234, 247, 265 and 267 cm^{-1}. Each component corresponds to one type of nanotube. Using d_t (nm) = 223.5/[ω_{RBM} (cm^{-1}) − 12.5], which can be applied to nanotubes in bundles [23], nanotube diameters were determined to be in the range from 0.88 to 1.17 nm. RBM peak positions, corresponding SWNT diameters and other properties are listed in Table 2. Change in 233 cm^{-1} band intensity with solvent δ_p values is plotted in Fig. 6. Here 233 cm^{-1} band intensity has been normalized to G band intensity. For $\delta_{p\text{-solvent}} < \delta_{p\text{-PMMA}}$, 233 cm^{-1} band intensity remains unchanged. For $\delta_{p\text{-solvent}} > \delta_{p\text{-PMMA}}$, 233 cm^{-1} band

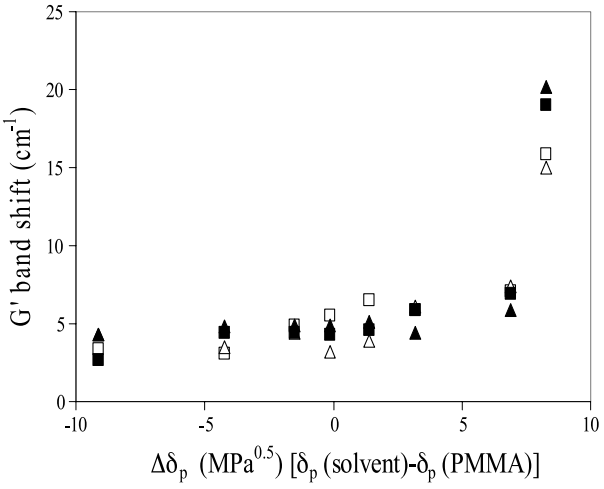

Fig. 4. G′ band shift in the PMMA/SWNT composites as a function of $\Delta\delta_p$ (the symbols have been defined in Fig. 3).

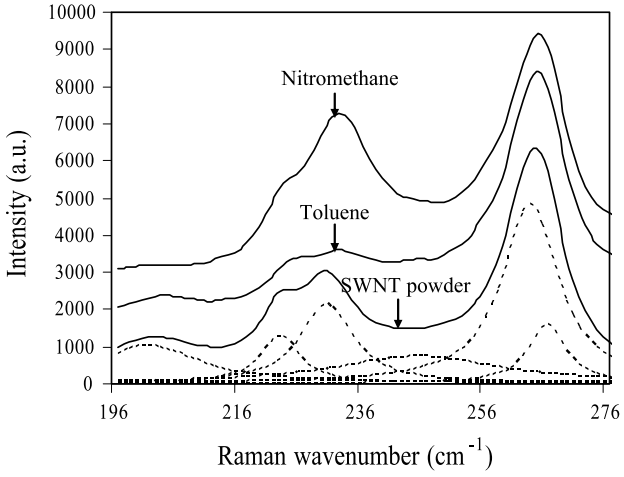

Fig. 5. RBM bands of SWNT powder and PMMA/SWNT composite films made from toluene and nitromethane. Dotted lines shown Lorentzian peak fitting to the SWNT powder spectra.

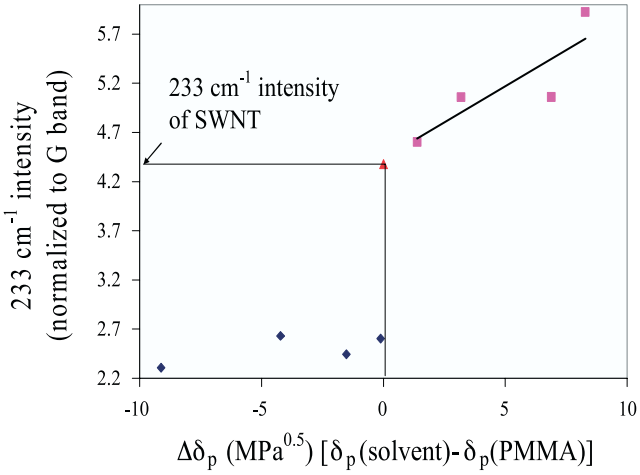

Fig. 6. 233 cm^{-1} band intensity in the composites as a function of $\Delta\delta_p$.

intensity increases with increasing solvent δ_p. Same trend was observed if RBM band intensity is normalized to the totally intensity of 265 and 267 cm^{-1} peaks.

The RBM intensity variations in PMMA/SWNT composites result from the effect of compressive strain on resonance. SWNT electronic band structure is modified under strain. This affects resonance condition as E_{ii} shifts closer to or further away from E_{laser}. The RBM intensity increases when the difference $|E_{ii}-E_{laser}|$ decreases and vice versa. The RBM intensity is maximum when E_{ii} is equal to E_{laser}. For $r=-1$ (see footnote of Table 2 for the definition of r), E_{22}^{s} decrease under compressive strain and increase for $r=1$. Under compressive stress, E_{22}^{s} increases for 265 cm^{-1} peak and decreases for 267 cm^{-1} peak and their energy values are relatively far from E_{laser}. Therefore, the other peak intensities can be normalized to the total intensity of these two peaks. E_{22}^{s} of 203 cm^{-1} decreases under compression and for the samples processed in nitromethane, the compressive force is highest. Thus E_{22}^{s} shifts farther away from E_{laser} (1.58 eV), and the peak almost disappears for PMMA/SWNT processed in nitromethane. E_{22}^{s} of 233 cm^{-1} band is between 1.59 and 1.67 eV (its theoretical value is 1.59 eV). With compressive strain this energy value decreases and shifts closer to the laser energy value of 1.58 eV. This enhances resonance, and results in increased intensity for the 233 cm^{-1} peak for those samples exhibiting homogeneous SWNT dispersion in PMMA.

4. Conclusions

SWNT dispersion in PMMA improved with increasing polar component of the solvent solubility parameter (δ_p), and the most uniform dispersion was obtained in nitromethane, which is the most polar solvent employed in this study. Composite films made from different solvents exhibited different degrees of dispersion, resulting in different compressive strains on the SWNT. Samples exhibiting poor dispersion as characterized by optical and scanning electron microscopic techniques resulted in no compressive strains. As the SWNT dispersion in polymer improved, compressive strain increased as monitored from

Table 2
The SWNT diameters corresponding to the observed Raman RBM peaks, van Hove transition energy E_{22}^{s}, change in transition energy E_{22}^{s} under compressive strain, and nanotube structural parameters (n, m) and r

ω_{RBM} (cm^{-1})	d_t (nm)	E_{22}^{s} (eV)[a][24]	E_{22}^{s} (eV)[b]	(n, m)	r	Change in E_{22}^{s} under compressive force
203	1.17	1.40–1.46	1.37	11, 6	−1	Decrease
226	1.05	1.53–1.60	1.54	10, 5	−1	Decrease
233	1.01	1.59–1.67	1.59	12, 1	−1	Decrease
247	0.96	1.70–1.79	1.84	10, 3	1	Increase
265	0.89	1.81–1.88	1.85	7, 6	1	Increase
267	0.88	1.81–1.90	1.78	10, 2	−1	Decrease

(n, m) are tube chiral vectors, $n-m=3q+r$, where q and r are integer values, change in E_{22}^{s} is based on tight binding calculations of Lucas and Young [25], where it has been shown that the change in Van Hove singularities under uniaxial strain depends on the nanotube structure.

[a] From Ref. [23].

[b] Calculated value [13].

changes in RBM intensity, as well as up shifts of both the G and G′ Raman bands.

Acknowledgements

The project was supported by the Office of Naval Research (N00014-01-1-0657), Air Force Office of Scientific Research (F49620-03-1-0124) and Carbon Nanotechnologies Incorporated. Useful discussions with Dr Tetsuya Uchida are gratefully acknowledged.

References

[1] Dresselhaus MS, Dresselhaus G, Avouris Ph. Carbon nanotubes: synthesis, structure, properties and applications. Springer series in topics in applied physics. vol. 80. Berlin: Springer; 2001.
[2] Bethune DS, Klang CH, de Vries MS, Gorman G, Savoy R, Vazquez J, et al. Nature 1993;363:603–7.
[3] Iijima S, Ichihashi T. Nature 1993;363:603–5.
[4] Baughman RH, Zakhidov AA, Heer WA. Science 2002;297:787–92.
[5] Shofner ML, Rodriguez-Macias FJ, Vaidyanathan R, Barrera EV. Compos Part A: Appl Sci Manuf 2003;34(12):1207–17.
[6] Sreekumar TV, Liu T, Min BG, Guo H, Kumar S, Hauge RH, et al. Adv Mater 2004;16(1):58–61.
[7] Kumar S, Dang TD, Arnold FE, Bhattacharyya AR, Min BG, Zhang X, et al. Macromolecules 2002;35(24):9039–43.
[8] Sen R, Zhao B, Perea D, Itkis ME, Hu H, Love J, et al. Nano Lett 2004;4(3):459–64.
[9] Benoit JM, Corraze B, Lefrant S, Blau WJ, Bernier P, Chauvet O. Synth Met 2001;121(1–3):1215–6.
[10] Sandler JKM, Kirk JE, Kinloch IA, Shaffer MSP, Windle AH. Polymer 2003; 44(19): 5893–5899.
[11] Liu T, Kumar S. Nano Lett 2003;3(5):647–50.
[12] Dresselhaus MS, Dresselhaus G, Jorio A, Filho GS, Saito R. Carbon 2002;40(12):2043–61.
[13] Kataura H, Kumazawa Y, Maniwa Y, Umezu I, Suzuki S, Ohtsuka Y, et al. Synth Met 1999;103(1–3):2555–8.
[14] Sandler J, Shaffer MSP, Windle AH, Halsall MP, Montes-Mora'n MA, Cooper CA, Young RJ. Phys Rev B 2003;67:035417.
[15] Dharap P, Li Z, Nagarajaiah S, Barrera EV. Nanotechnology 2004; 15(3):379–82.
[16] Cooper CA, Young RJ, Halsall M. Compos Part A: Appl Sci Manuf 2001;32(3-4):401–11.
[17] Venkateswaran UD, Gosselin M-É, Postek B, Masica DL, Chen G, Gupta R, et al. Phys Status Solidi B 2003;235(2):364–8.
[18] Huang F, Yue K, Tan P, Zhang S, Shi Z, Zhou X, et al. J Appl Phys 1998;84(7):4022–4.
[19] Hummer G, Rasaiah JC, Noworyta JP. Nature 2001;414:188–90.
[20] Ci L, Zhou Z, Song L, Yan X, Liu D, Yuan H, et al. Appl Phys Lett 2003;82(18):3098–100.
[21] Li HD, Yue KT, Lian ZL, Zhan Y, Zhou LX, Zhang SL, et al. Appl Phys Lett 2000;76(15):2053–5.
[22] Li Z, Dharap P, Nagarajaiah S, Barrera SV, Kim JD. Adv Mater 2004; 16(7):640–3.
[23] Bachilo SM, Strano MS, Kittrell C, Hauge RH, Smalley RE, Weisman RB. Science 2002;298:2361–6.
[24] Dresselhaus MS, Eklund PC. Adv Phys 2000;49(6):705–814.
[25] Lucas M, Young RJ. Phys Rev B 2004;69:085405.
[26] Brandrup J, Immergut EH, Gurlke EA, editors, Polymer Handbook, IVth edition, John Wiley and Sons, New York, 1999.